Experimental and Analytical Investigation of Steel Beams Rehabilitated Using GFRP Sheets

A. A. El Damatty*, M. Abushagur, M. A. Youssef
Department of Civil and Environmental Engineering, The University of Western Ontario, London, ON, CANADA, N6A 5B9

Abstract

Aging and deterioration of existing steel structures necessitate the development of simple and efficient rehabilitation techniques. The current study investigates a methodology to enhance the flexural capacity of steel beams by bonding Glass Fibre Reinforced Plastic (GFRP) sheets to their flanges. A heavy duty adhesive, tested in a previous study is used to bond the steel and the GFRP sheet. In addition to its ease of application, the GFRP sheet provides a protective layer that prevents future corrosion of the steel section. The study reports the results of bending tests conducted on a W-shaped steel beam before and after rehabilitation using GFRP sheets. Enhancement in the moment capacity of the beam due to bonding GFRP sheet is determined from the test results. A closed form analytical model that can predict the yield moment as well as the stresses induced in the adhesive and the GFRP sheets of rehabilitated steel beam is developed. A detailed finite element analysis for the tested specimens is also conducted in this paper. The steel web and flanges as well as the GFRP sheets are simulated using three-dimensional brick elements. The shear and peel stiffness of the adhesive are modeled as equivalent linear spring systems. The analytical and experimental results indicate that a significant enhancement in the ultimate capacity of the steel beam is achieved using the proposed technique. The finite element analysis is employed to describe in detail the profile of stresses and strains that develop in the rehabilitated steel beam.

Keywords: Rehabilitation, Steel beams; Glass Fibre Reinforced Plastic; Experimental; Finite Element; Analytical Model

* Corresponding author. Tel.: 1-519-661-2111 Ext. 88203, Fax: 1-519-661-3779
E-mail address: damatty@uwo.ca (A.A. El Damatty)

1. Introduction

The deterioration of steel structures due to corrosion and aging necessitates the development of simple and practical techniques to rehabilitate such structures. In the past two decades, fibre reinforced plastics (FRP) have been extensively used to rehabilitate concrete structures. This has included the strengthening of beams (Mettemeyer et al., 1999), columns (Priestly et al., 1992), shear walls (Lombard et al., 1999) and bridges (Roberts, 1997). A noticeable increase in strength and/or ductility of the concrete elements was shown in these applications. The main advantages of FRP are their high strength-to-weight ratio and their excellent resistance against corrosion and chemical attacks. New uses of FRP to upgrade the resistance of steel structures have recently been expressed in the civil engineering consulting community. An advantage of this specific type of composite construction is the ease of application using a heavy adhesive system to bond the FRP and the steel elements. Wang (1992) studied experimentally and analytically the use of carbon fibre reinforced polymer laminates (CFRP) in the repair of composite steel bridge members. The study showed that rehabilitating steel beams using CFRP plates was effective as it resulted in a 21.58% to 41.60% increase in the ultimate flexural capacity. The analytical model was based on a perfect bond between the steel and the CFRP plates and thus was limited to specific cases where the discontinuity between the steel beam and the CFRP plate introduced by the bonding agent has minor effects. Sen et al. (2001) and Liby (1993) extended Wang's experimental study to include specimens initially loaded past their yield strength. They estimated that the increase in the flexural capacity ranged between 11% and 50%. Their experiments indicated that for relatively thick bonded laminates, failure occurred in the epoxy adhesive that was used to bond the steel and the plastic sections. As such, the success of this technique relies largely on the behaviour of the bonding adhesive. El Damatty and Abushagur (2003) have recently investigated the shear and peeling behaviour of Glass Fibre Reinforced plastics (GFRP) bonded to steel sections. A preliminary investigation was conducted to select the type of adhesive that would be suitable for such an application and it led to a methacrylate adhesive system commonly used in the car and bus

manufacturing industries. The same chemical product was also used by Chakrabati and Mosallam (1998) in their study that involved bonding polymer composite stiffeners to steel beams. A large number of shear lap tests was conducted by El Damatty and Abushagur (2003) and the failure loads, displacements and strains were recorded. A mathematical model in which the shear and peel stiffness of the adhesive were represented as two continuous linear spring systems was developed and the results of the tests were incorporated into this mathematical model to determine the constants of the spring systems.

The use of GFRP has many advantages including the following: a) much lower cost compared to carbon fiber composites, b) ease of handling due to its light weight, c) ease of application through bonding to the steel using heavy duty adhesive, and d) creation of a corrosion protective layer for the steel. The current study investigates experimentally and analytically the use of GFRP sheets to upgrade the flexural resistance of steel beams. One of the major objectives is to assess the ability of the adhesive to transfer the load between the steel and plastic media. GFRP sheets were bonded to both the upper and lower flanges of a steel beam. The same methacrylate adhesive system tested previously by El Damatty and Abushagur (2003) was used to bond the GFRP and the steel sections. The rehabilitated beam was then subjected to a two-point loading that results in a state of pure bending at the middle part of the beam. The increase in both the yield and the ultimate moment capacities of the beam due to the addition of the GFRP sheets was assessed experimentally and a closed form analytical model that describes the bending behaviour of the steel/GFRP section up to yielding was developed. The adhesive connecting the plastic and the steel components was simulated in this model as a linear spring system with properties based on the results of the study conducted by El Damatty and Abushagur (2003). The experimental results were used to validate this mathematical model. This model can be easily employed to estimate the yield moment and the corresponding stresses that develop in the steel, plastic and adhesive media. In order to understand the post-yield behaviour, a three-dimensional finite element model that simulates the bending test of

the rehabilitated beam was also developed. The failure mode of the rehabilitated beam was identified by comparing the finite element to the test results.

2. Experimental Program

The flexural performance of a W150x37 steel beam before and after strengthening by bonding GFRP sheets to its top and bottom flanges was investigated experimentally. One reference steel beam (B1) and two rehabilitated beams (B2 and B3) with exactly similar configurations were tested. Fig. 1, 2a and 2b show a photo of the test setup, a schematic of the test and a cross-section of the tested specimen, respectively. As shown in Fig. 2a, the steel beams are simply supported at their two edges and have a span L_b = 2800 mm. The yield stress (σ_y) and modulus of elasticity (E_s) of the steel beam were determined by testing two coupons; one taken from the flange and the other taken from the web. For both coupons, a rectangular piece of steel was flame cut from the tested beam and then machine cut to the dimensions shown in Fig. 2c. Both tested coupons resulted in exactly the same σ_y (363 MPa) and E_s ($2x10^5$ MPa).

2.1. GFRP sheets

The GFRP sheets were supplied by the manufacturer in large panels of length 2.4 m, width 1.2 m and thickness 19 mm. They were cut in strips 154 mm wide (to match the steel beam width) and 2400 mm long (L_f) in the machine shop at The University of Western Ontario. The plates are manufactured using the pultrusion process and consist mainly of a large number uni-directional layers that provide strength and stiffness in the longitudinal direction. The laminate includes only four layers of randomly oriented mat fibers that provide strength in the transverse direction in order to protect the plate from shipping, cracking and linear fracturing. A polyester peel-ply layer covered each side of the GFRP sheets. A tensile test was conducted for one of the GFRP plates to determine its tensile strength and modulus. Values of 206.85 MPa for tensile strength and $17.2x10^3$ MPa for modulus of elasticity resulted from this test.

2.2. Adhesive

One of the main challenges in a rehabilitation technique such as this is the choice of a heavy duty adhesive system to bond the steel and the plastic materials. El Damatty and Abushagur (2003) found that the best level of bond between steel and GFRP sheets could be achieved using a methacrylate adhesive system (A0420) and this product was adopted for use in the current study. According to El Damatty and Abushagur (2003), the average values for the constants of the linear continuous springs simulating the shear and peel stiffness of this adhesive were equal to 21.79 N/mm^3 and 2.26 N/mm^3, respectively. These values are associated with the optimum adhesive thickness (0.79 mm) specified by the manufacturer. This thickness was also applied in the flexural tests performed in the current study. The shear strength of this product is about 24 MPa, based on the information provided by the manufacturer. However, in some of the shear lap tests conducted by El Damatty and Abushagur (2003), a shear strength value of 35 MPa was reached.

2.3. Rehabilitating the steel beams

Two steel beams (B2 and B3) were rehabilitated using GFRP to assess the variability in the suggested method of rehabilitation. The rehabilitation process of the steel beams can be divided into three main steps:

1. Preparation of the W150x37 steel beams:
    a. The beams were sandblasted in order to remove any rust or grease.
    b. The surface was cleaned using alcohol methanol acid in order to remove any dirt.
    c. A primer was applied to the surface as recommended by the manufacturer.

2. Preparation of the GFRP sheets:
    a. The two non-structural layers of polyester non-woven fabric (peel-ply layers) that encase the GFRP for manufacturing purposes were removed.

b. The adherence face of the GFRP sheets was cleaned using alcohol methanol acid to avoid any contamination.

3. Bonding the GFRP sheets to the steel beams (The GFRP sheets covered almost the entire span of the rehabilitated beams with the exception of 20 mm near the two supports):

   a. The adhesive was applied to the GFRP sheets to a thickness of 0.79 mm as recommended by the manufacturer. The thickness of the adhesive was controlled using two longitudinal wires of 0.79 mm placed at interface between the steel flanges and GFRP sheets.

   b. The GFRP sheets were attached to the steel beams and then clamped using a C-clamp that was adjusted to obtain the proper adhesive thickness.

   c. The top level of the GFRP sheets was leveled to allow uniform distribution of the applied load.

   d. A hardening period of 15 days prior the testing was allowed in order that the adhesive reaches its maximum strength.

2.4. Test procedure and instrumentation

As shown in Fig. 2a, the load was transferred to the test specimens through a rigid load distributor in the form of two concentrated forces. The load was applied using a MTS hydraulic machine in a load-controlled manner for the elastic range at a rate of 2.0 kN/minute and a displacement-controlled manner for the plastic range at a rate of 0.5 mm/minute.

A LVDT was attached to the steel beam at its mid-span in order to measure the vertical displacement. In addition, the flexural strains occurring at various stages of loading were measured at mid-span of the beam. At this location, eight strain gauges were attached to the outer faces of the GFRP sheet and the inner faces of the steel section flanges. The locations of these strain gauges are shown in Fig. 2b.

3. Analytical Model

The purpose of this section is to develop a closed form analytical model that can predict the yield moment capacity of the rehabilitated steel beam. The model will also provide estimates of the stresses induced in the adhesive, the steel and the GFRP sections within the range of elastic behaviour. The stresses acting on an infinitesimal element (dx) of the GFRP plate are shown in Fig. 3a. σ and u_2 are the axial stresses and the axial displacements at a general point of the GFRP plate. These two quantities are assumed here to be constant within the thickness of the GFRP sheet. The shear stress τ that develops in the adhesive can be expressed by the following equation:

$$\tau = k_s(u_2 - u_1) \qquad (1)$$

where u_1 is the axial displacement at the extreme fibres of the steel section and k_s is the spring constant that simulates the shear stiffness of the adhesive that was evaluated experimentally by El Damatty and Abushagur (2003).

The differential equation that results from the equilibrium of forces of this infinitesimal element is shown below:

$$u_1 = u_2 - \frac{E_f t_f}{k_s}\frac{d^2 u_2}{dx^2} \qquad (2)$$

A typical distribution of axial stress along the depth of the steel/ GFRP section is provided in Fig. 3b.

The following relation is obtained by equating the external moment (M) to the internal moment that resulted from this stress distribution:

$$M = 2\frac{E_s I_s}{h}\frac{du_1}{dx} + b\,h_1 E_f t_f \frac{du_2}{dx} \qquad (3)$$

In the above equation b is the width of both the GFRP sheet and the steel flanges, E_s, I_s and h are the modulus of elasticity, the moment of inertia and the depth of the steel section, E_f and t_f are the

modulus of elasticity and the thickness of the GFRP sheet and h_1 is the distance between the centers of the top and bottom of the GFRP sheets.

By substituting Eq. (2) into Eq. (3) and replacing $v = \frac{du_2}{dx}$, the following differential equation is obtained:

$$M_1 = \omega^2 v - v'' \qquad (4)$$

where $M_1 = M\ c,$

$$c = \frac{k_s h}{2 E_s I_s E_f t_f},$$

and $$\omega^2 = \frac{k_s}{E_f t_f} + \frac{b\ h\ h_1\ k_s}{2\ E_s I_s}.$$

The particular solution of the above differential equation depends on the shape of the external moment (M). Therefore, two different regions are considered in the solution; region A between the two point loads where the moment (M) is constant and equal to M_0, and region B bounded by the loads and the ends of the GFRP section where the moment (M) varies linearly and can be written as:

$$M = \frac{2 M_0}{(L_b - L_p)}\left(\frac{L_b}{2} - x\right) \qquad (5)$$

where x is the distance from mid-span to the point of consideration.

The solution of Eq. (4) in both regions can be written as:

Region "A"

$$-\frac{L_P}{2} \le x \le \frac{L_P}{2}$$

$$v_A = A \sinh(\omega x) + B \cosh(\omega x) - \frac{M_0 C}{\omega^2} \qquad (6)$$

Region "B"

$$\frac{L_P}{2} \le |x| \le \frac{L_f}{2}$$

$$v_B = C \sinh(\omega x) + D \cosh(\omega x) - \frac{2 M_0 C}{\omega^2 (L_b - L_p)} \left(\frac{L_b}{2} - x\right) \quad (7)$$

The constants A, B, C and D can be evaluated by applying the following four boundary conditions:

1. $$\frac{dv_A}{dx}(x = 0) = 0 \quad (8)$$

2. $$v_A\left(\frac{L_p}{2}\right) = v_B\left(\frac{L_p}{2}\right) \quad (9)$$

3. $$\frac{dv_A}{dx}\frac{L_p}{2} = \frac{dv_B}{dx}\frac{L_p}{2} \quad (10)$$

4. $$v_A\left(\frac{L_F}{2}\right) = 0 \quad (11)$$

Eq. (8) reflects the symmetry of the problem about the centerline of the assembly. Eq. (9) and (10) simulate the continuity of strains and curvature between regions A and B. Eq. (11) describes the state of free stress at the free edges of the GFRP sheets. By applying the above boundary conditions, the four constants A, B, C and D can be evaluated for a certain value of applied moment M_0. These constants are back substituted into Eq. (6) and (7) to obtain the distribution of the GFRP strains $v = \frac{du_2}{dx}$ that develop in regions A and B.

Eq. (2) can be differentiated to obtain the strain $\frac{du_1}{dx}$ that develops at the extreme fibre of the steel section after substituting for $v(x) = \frac{du_2}{dx}$ and for $\frac{d^3u_2}{dx^3} = \frac{d^2v}{dx^2}$. By multiplying the strain functions $\frac{du_1}{dx}$ and $\frac{du_2}{dx}$ by E_s and E_f, respectively, the distribution of axial stresses that develops in the GFRP and the steel effect can be evaluated. Eq. (2) can be also applied to obtain the relative axial displacement (u_2- u_1) that occurs between the GFRP and the steel section after

substituting $\frac{d^2 u_2}{d x^2} = \frac{dv}{dx}$. Multiplying the relative displacement by k_s leads to an evaluation of the distribution of sheer stresses that develops in the adhesive. The location and magnitude of the maximum values for the axial stresses in both the steel and the GFRP sections as well as the maximum shear stresses in the adhesive can be then obtained. The yield moment M_y of the rehabilitated sections is governed by one of the following criteria:

a) the maximum stress in the steel section reaches $\sigma_{y;}$
b) the maximum stress in the GFRP reaches the ultimate capacity of the composite material; and
c) the maximum shear stress in the adhesive exceeds its shear strength.

Disadvantages of this analytical approach include its limitation to the prediction of the linear behaviour of the composite beam up to the yield moment and its inability to capture the peeling behaviour of the adhesive. However, it provides a quick estimate of the yield moment capacity of the rehabilitated section and can be used to conduct a parametric study to investigate the effect of various parameters.

4. Finite Element Modeling

Detailed three-dimensional finite element modeling was conducted for the specimens tested here. The model was developed using the commercial finite element program ANSYS (revision 5.3). In order to capture the local effects, the flanges and the web of the steel beam as well as the GFRP sheets were simulated using three-dimensional brick elements; namely the eight nodes solid element. The following features were included in the finite element model:

1. The double node concept was applied at the interface between the steel and the GFRP faces. For each nodal point of the steel flanges located at the interface, a corresponding node exists at the GFRP part having exactly similar coordinates. No compatibility in displacements is applied between these two conjugate nodes.

2. The adhesive was simulated using a three-dimensional continuous spring system located at the interface between the steel and the GFRP parts that connect the conjugate nodes. The spring constant in the plane of the flange (k_s) simulates the shear stiffness of the adhesive while the spring constant in the direction normal to flanges k_p represents the peel stiffness of the adhesive. Values of these spring constants were assumed to be equal to the average values obtained from the shear lap tests conducted by El Damatty and Abushagur (2003). Therefore, $k_s = 21.79$ N/mm^3 and $k_p = 2.26$ N/mm^3.
3. The analysis included the geometric and material non-linear effects. As such, the model can predict the delay in flange local buckling due to the addition of GFRP plates. A bilinear isotropic hardening model was used for the steel part. Based on the results of the coupon tests, the tangent modulus was assumed to be equal to 3% of the elastic modulus. Due to its brittle behaviour, only a linear elastic model was assumed for the GFRP followed by a sudden failure when the ultimate stresses were reached. The non-linear analysis was conducted incrementally in a load-control manner. A typical finite element mesh for the beam assembly is shown in Fig. 4.

5. Experimental Results

The experimental results showed a near perfect match in the performance of specimens B2 and B3. The differences in loads and displacements between the two specimens did not exceed one percent. This indicates that the proposed rehabilitation technique is reliable. Only specimen B2 will be addressed in the following discussion.

The load-deflection curves that resulted from the bending tests of specimens B1 (without GFRP) and B2 (with GFRP) can be found in Fig. 5. In these curves, the vertical axis represents the total load applied by the MTS machine, while the x-axis represents the corresponding deflection measured at the mid-point of the beam. At any load state, the constant moment acting at the middle region of the beam is given as:

$$M = P * (L_b - L_p)/4 \quad (12)$$

The following observations can be drawn by comparing the load-deflection curves resulting from the two bending tests:

1) For specimen B1, yielding of the extreme fibres of the steel section started at a load of 208.97 kN. The corresponding yield moment M_y, based on Eq. (12) is equal to 97.52 kN.m. The calculated value for the yield moment based on the relation $M_y = S * \sigma_Y$ almost matches the above value (99.46 kN.m.). At a load value of 243.43 kN (moment = 113.60 kN.m), full yielding of the steel section occurred. At this point, the section reached its plastic moment capacity and no increase in the moment was observed beyond this value. The corresponding plastic moment M_p of the section, calculated from section capacity, ($Z* \sigma_Y$), is equal to 112.53 kN.m. Since no increase in load carrying capacity was observed beyond the plastic moment, the ultimate moment capacity of the section M_u was considered to be equal to its plastic capacity M_p.
2) The load-deflection curve that resulted from testing specimen B2 showed linear behaviour up to a load of 257.61 kN (Moment = 120.22 kN.m). As expected, a slightly higher value for the elastic stiffness was exhibited by the strengthened section. A transitional region characterized by a variation in the load-deflection slope and consequently the stiffness was shown in a load range that varied between 257.61 kN and 302.80 kN. It is anticipated that yielding at the extreme fibres of the steel section started at 257.61 kN and that the steel section fully yielded at 302.80 kN. Since GFRP materials experience a brittle type of failure, it is expected that up to the total failure of the specimen, the stresses in the GFRP plate were less than its ultimate strength. Beyond 302.80 kN, Fig. 5 indicates that the section has a positive stiffness (about 15% of the pre-steel yielding stiffness) and has the ability to carry extra loads. In this region, the stiffness of the section results only from the contribution of the GFRP plates. Specimen B2 failed at a load equal to 432.80 kN (moment = 201.97 kN.m). Delamination between the layers of the bottom GFRP sheet was observed during the failure. A photo showing the initiation of failure is illustrated in Fig. 6. It was not clear if the

failure was initiated due to delamination or due to excessive tensile stresses of the composite material. The failure mode was assessed in view of the finite element results that are presented later. No sign of failure at the interface between the GFRP and the steel materials was observed up to this load confirming the excellent bond provided by the adhesive. The yield moment capacity M_y of the rehabilitated beam was defined as the value at which yield initiates in the steel section, while its ultimate capacity M_u was defined as the value at which the specimen fails. Based on the experimental results, specimen B2 achieved values for yield moment and ultimate moment capacities equal to 120.22 kN.m. and 201.97 kN.m., respectively.

3) The experimental results indicated that the addition of the 19 mm GFRP plates led to an increase of the load value at which the steel section started to yield (and consequently M_y) by approximately 23%. Based on an assumption of full compatibility at the interface between the GFRP and the steel parts, the GFRP plates can be substituted with steel plates with thickness $e_{quivalent} = t_f/n$, where n is the ratio between the steel and the GFRP modulus of Elasticity, i.e. $n = E_s/E_f$. Based on this assumption, the increase in the yield moment capacity of the steel section should be about 21%. This value is very close to the experimental findings. This indicates that the presence of an elastic medium in the form of adhesive did not significantly alter the behaviour of the section.
4) The addition of the GFRP plates has increased the ultimate capacity of the beam by about 78%. The observed increase in both the post yield strength and stiffness is expected to result in higher post yield energy dissipation.

The load-strain curves recorded during testing of specimen B2 by strain gauges S6 (recording the GFRP strains) and S4 (recording the steel strains) are shown in Fig. 7a and 7b, respectively. The GFRP load-strain curve (S6) is linear up to a load of 257.61 kN. At this point, the extreme fibres of the steel section yielded and the GFRP started to have an increasing share in resisting load. The GFRP share reached 100% at a load of 302.80 kN which defines the full yielding of the steel

section. The steel load-strain curve (S4) is linear up to a load of 282.22 kN which defines the point of full yielding of the steel beam flanges. The accuracy of these strain measurements was verified by the almost equal measurements for the two strain gauges attached at the same vertical level. Also, the strains measured at the compression flange were almost equal and opposite in sign to the corresponding ones measured at the tension flange. An attempt was made to measure the strains at the interface between the GFRP and the steel sections, but failed and therefore measurements were not included.

6. Comparison Between Analytical, Numerical and Experimental Results

The developed analytical model can describe the behaviour of the composite beam within the elastic limit of the steel section. Meanwhile, the non-linear three-dimensional finite element model can predict this behaviour within as well as beyond the elastic limit. The values of M_y for specimen B1 and B2 predicted experimentally, as well as analytically and numerically are provided in Table 1. The values predicted by these three different procedures almost match. This provides a validation for the analytical model as well as confidence in the accuracy of the finite element model. The maximum stresses that developed in the GFRP plates at yielding were evaluated using both the analytical and the finite element models as well as experimentally and are provided in Table 2. These values indicate that when the extreme fibres of the steel section yielded, the stresses in the GFRP section were well below (about one fifth) their ultimate values. The corresponding values for adhesive shear stresses are provided in the same table indicating that these are less than the shear strength of the adhesive. Again, the agreement between the models and the experimental results is excellent.

The ultimate capacities of specimen B1 ($M_u = M_p$) based on both the finite element and the experimental results are given in Table 1. The difference between the results predicted using the two approaches is almost negligible. The comparison between the numerical and experimental predictions for ultimate moment capacities will be discussed together with the failure mode later on

in this study. In order to compare to the experimental results, the load deflection curves predicted by the finite element analysis for beams B1 and B2 are plotted in Fig. 5 with the corresponding curves obtained experimentally. The two curves show almost a perfect match.

7. Distribution of Stresses Based on the Finite Element Results

The validated finite element model was used to predict some parameters that were difficult to evaluate experimentally for the rehabilitated beam. These included the distribution of flexural strains and stresses along a cross-section of the beam with the discontinuity expected to occur at the interface between the steel and the GFRP sheets, the distribution of sheer and peel stresses in the adhesive, and the distribution of axial stresses in the GFRP plates.

Fig. 8 provides the distribution of flexural stresses at the mid-span of the beam in both the elastic (P=150 kN) and the inelastic (P=350 kN) ranges. The corresponding distribution of flexural strains is given in Fig. 9.

The figure show a linear distribution of flexural strains in both the elastic and the inelastic ranges with a small jump of strain values at the interface between the steel and the GFRP sheet. The modulus of the steel part exceeds the modulus of the GFRP element during the elastic range and therefore a reduction in the GFRP strains was observed at the interface. During the inelastic range, the modulus of the GFRP exceeds the effective modulus of steel and as a result this effect was reversed.

A linear stress distribution is shown in both the steel and the GFRP sections within the elastic range. Due to the large difference in the elastic modulus, the GFRP stresses were much smaller than the steel ones. In the inelastic range, the steel section has almost fully yielded while the stresses in the GFRP part have significantly increased as it carries the extra loads once the steel yields.

The distribution of axial displacement (u_1) at the extreme fibres of the steel section as well as the distribution of axial displacement (u_2) at the inner surface of the GFRP sheets was predicted at various loading stages by the finite element analysis. Eq. (1) was applied to obtain the distribution

of shear stresses that develop in the adhesive. This distribution is provided in Fig. 10 for the adhesive connecting the bottom flange and the GFRP sheet for both the elastic and the inelastic ranges of behaviour. A comparison between the two plots shown in the figure indicated that the maximum shear value varied non-linearly with the applied load. An increase in the load by a ratio of 2.3 led to an increase in the maximum shear stress by approximately a ratio of 3.6. The distribution of shear stresses is anti-symmetric during the two loading stages. The change in sign of the distribution during the elastic and the inelastic ranges reflects a change in the sign of the relative displacements at the interface of the steel and the composite sections. This is due to the variation of relative stiffness between the two materials before and after the yielding of the steel part. In the elastic range, the maximum shear stresses occur at the end of the GFRP sheet. In the inelastic range, the stress profile is close to the distribution of shear forces acting on the beam with a zero value between the loads and a constant value elsewhere.

Similarly, the finite element analysis provided an evaluation for the distribution of the vertical deflections w_1 and w_2 at the extreme steel fibres and the inner faces of the GFRP sheets. The difference between these two deflection curves (Δw) represents the relative vertical deflection at the interface that results from the out-of-plane deformation of the adhesive. By multiplying Δw by the spring constant K_p, that simulates the peel stiffness of the adhesive and has a value of 2.26 N/mm^3 (El Damatty and Abushagur, 2003), the distribution of peel stresses along the length of the GFRP sheet can be evaluated. This distribution is provided in Fig. 11 for the adhesive connecting the bottom flange and the GFRP sheet both the elastic and inelastic ranges of behaviour. The distribution shows a symmetric behaviour about the center of the beam. In this figure, a negative value indicates stresses causing expansion of the adhesive and consequently a tendency of separation between the steel and the plastic sections. It is clear from the plots that critical locations for peel failure are towards the edges of the GFRP sheet.

The distributions of axial stresses at the extreme fibres of the GFRP sheets for both the elastic and the inelastic ranges are provided in Fig. 12 for the bottom GFRP sheet. In the inelastic range, when

the load is carried mainly by the GFRP sheets, the distribution matches in shape the bending moment diagram.

8. Prediction of Failure Mode Based On Test's Observation and Finite Element Results

As shown in Fig. 6, the failure was initiated at the bottom GFRP sheet in the middle region of the beam between the points of application of the loads. No failure was observed in the adhesive. The failure of the GFRP sheet could occur as the result of one of two reasons:

a) The axial stresses reach the maximum tensile strength of the composite material.
b) Delamination between the GFRP layers due to either shear or peel failure occurs between the layers.

At any point inside the GFRP sheet, the inter-laminar shear and peel stresses are expected to vary linearly within the thickness of the sheet with maximum values at the interface with the steel section and zero values at the outer face of the sheet. The longitudinal distribution of these stresses is expected to follow the patterns given in Fig. 10 and 11. Fig. 10 indicates that the maximum value of shear stresses is not located between the point loads. Also, as mentioned earlier, Fig. 11 indicates that the edge of the GFRP sheet represents the critical location for inter-laminar peel failure. Therefore, one would rule out the possibility that delamination failure was initiated at the location of maximum moment between the two points load. On the other hand, Fig. 12 indicates that the maximum tensile stresses in the GFRP sheet occur between the two loads. As such, it can be concluded that tensile failure of the GFRP bottom sheet initiated the collapse of specimen B2.

9. Conclusions

An experimental-analytical investigation was conducted to develop an understanding of the behaviour of steel beams rehabilitated using GFRP. In the experimental study, a methacrylate adhesive system was used to bond 19 mm GFRP sheets to the top and bottom flanges of a W157x17 steel beam. The assembly was tested under a state of pure bending. The results were compared to a similar test of an un-rehabilitated steel beam. A closed form analytical solution for the flexural

behaviour of the rehabilitated beams within the elastic range was derived. A three-dimensional nonlinear finite element model of the steel/GFRP assembly was also developed to simulate the behaviour in both the pre- and post-yielding stages.

In general, the comparison between the experimental, analytical and finite element results showed excellent agreement that validated the developed tools. In view of these results, the following conclusions could be drawn:

1. The addition of the GFRP sheets provided an increase of about 15%, 23% and 78% in the initial stiffness, yield moment and ultimate moment of the steel beam, respectively. The significant increase in the moment capacity, especially the ultimate one, made this technique promising for various applications.
2. At the interface between the GFRP and the steel surfaces, a discontinuity in strains was observed as a result of the flexibility of the adhesive media. Within the elastic range, the strains in the steel flange were slightly higher than those in the GFRP sheet. This behaviour was reversed when the steel yielded and its modulus became much lower than the GFRP modulus.
3. The longitudinal distribution of the adhesive shear stresses was anti-symmetric, having a linear variation prior to steel yielding and a variation matching the shear force diagram after steel yielding.
4. The longitudinal distribution of the adhesive peel stresses was symmetric with maximum values occurring at the edges of the GFRP sheets.
5. The longitudinal distribution of axial stresses developing in the GFRP sheets was symmetric. The distribution followed the bending moment diagram when the steel section reached the fully yielded stage.
6. No failure was observed at the interface between the GFRP and the steel face indicating excellent performance of the adhesive.

7. It is anticipated that the failure was triggered by the GFRP sheet reaching its maximum tensile strength capacity.

A more detailed numerical modeling is needed in order to be able to predict inter-laminar stresses within the GFRP plates. Also thermal analysis is suggested in order to investigate the effect of mismatch in the thermo-elastic properties between the steel and the GFRP at the interface.

Nomenclature

b Width of both the GFRP sheet and the steel flanges

E_f Modulus of elasticity of the GFRP sheet

$e_{quivalent}$ GFRP sheet equivalent steel plate

E_s Steel modulus of elasticity

H Depth of the steel beam

h_1 Distance between the centers of the top and bottom of the GFRP sheets

I_s Moment of inertia of the steel beam

k_p Spring constant that simulates the peel stiffness of the adhesive

k_s Spring constant that simulates the shear stiffness of the adhesive

L_b Span of the steel beam

L_f GFRP sheet length

M External moment

M_p Plastic moment

M_u Ultimate moment capacity of the section

M_y Yield moment

n Ratio between the steel and the GFRP modulus of Elasticity

t_f Thickness of the GFRP sheet

u_1 Axial displacement at the extreme fibres of the steel section

u_1 Axial displacement at the extreme fibres of the steel section

u_2 Axial displacement at the inner surface of the GFRP sheets

u_2 GFRP sheet axial displacements

w_1 Vertical deflection of the extreme steel fibres

w_2 Vertical deflection of the inner faces of the GFRP sheet

x Distance from beam mid-span to the point of consideration.

Δw Relative vertical deflection at the interface

σ GFRP sheet axial stresses

σ_y Steel yield stress

τ Adhesive shear stress

Acknowledgement

The authors would like to acknowledge the financial support provided to this project by the Natural Sciences and Engineering Research Council of Canada (NSERC) and the in-kind support provided by Plexus Canada through the donation of the adhesive used in this study.

References

- ANSYS program revision 5.3. ANSYS Inc., Canonsburg, PA.
- Chakrabarti P.R. and Mosallam A.S., (1998), "Performance of welded steel beam-to-column joints seismically retrofitted with polymer & steel stiffeners", Proceedings of the 2nd international conference on composites in infrastructure, Tucson, AZ, USA.
- El Damatty, A. and Abushagur, M., (in press), "Testing and modeling of shear and peel behaviour for bonded steel/FRP connections", J. of thin walled structures, Accepted Jan. 2003.
- Liby L.W., (1993), "Steel composite bridge sections strengthened by carbon fibre reinforced plastic laminates", Master of Science in engineering thesis, University of South Florida.

- Lombard, J.C.; Lau, D.T. and Foo, S., (1999), "Experimental study of reinforced concrete shear walls strengthened with fibre reinforced plastic sheets" Proceedings of the 8th Canadian conference, Canadian association for earthquake engineering, Vancouver, BC, 543-548.
- Mettemeyer, M.; Serra, P.; Wuerthele, M.; Schuster, G. and Nanni, A. (1999), "Shear load testing of carbon fibre reinforced polymer strengthened double tee beams in precast parking garage", Proceedings of the 4th international symposium on fibre reinforced polymer reinforcement for concrete structures, ACI SP-188, Baltimore, MD, 1063-1072.
- Priestly, M.J.N.; Seible, F. and Fyfe, E., (1992) "Column seismic retrofit using fiberglass/epoxy jackets", Proceedings of the 1st international conference on advanced composite materials in bridges and structures, Sherbrooke, QC, 287-299.
- Roberts J.E., (1997), "Application of composites in California bridges", Proceedings of structures congress (XV), The structural engineering institute, ASCE, Portland, OR, 56-66.
- Sen, R.; Liby, L. and Mullins, G., (2001), "Strengthening steel bridge sections using CFRP laminates", Journal of composites, B (32), 309-322.
- Wang, Y., (1992), "Bridge strengthening using advanced composites", Master of Science in Engineering thesis, University of South Florida.

Table 1: Experimental, Analytical and Finite Element Results

Method	B1		B2	
	M_y (kN.m.)	M_u (kN.m.)	M_y (kN.m.)	M_u (kN.m.)
Experimental	97.52	113.60	120.22	201.97
Analytical	99.46	112.53	119.97	---
Finite Element	99.80	112.85	118.00	198.54

Table 2: Maximum GFRP and Adhesive Stresses at Steel Yielding

Method	GFRP Stress at Yielding (MPa)	Adhesive Stress at Yielding (MPa)
Experimental	40.21	-----
Analytical	41.30	13.18
Finite Element	43.64	12.17

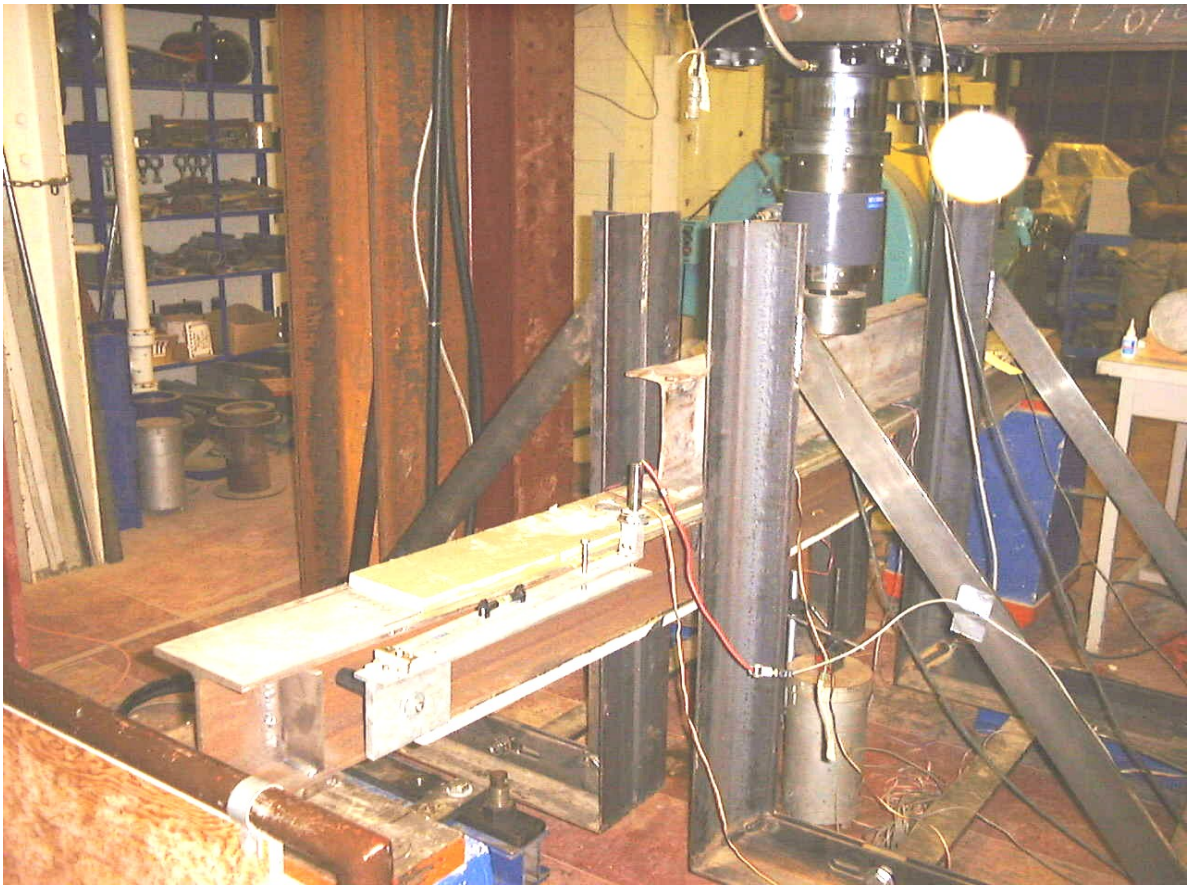

Figure 1 Photo of Test Setup

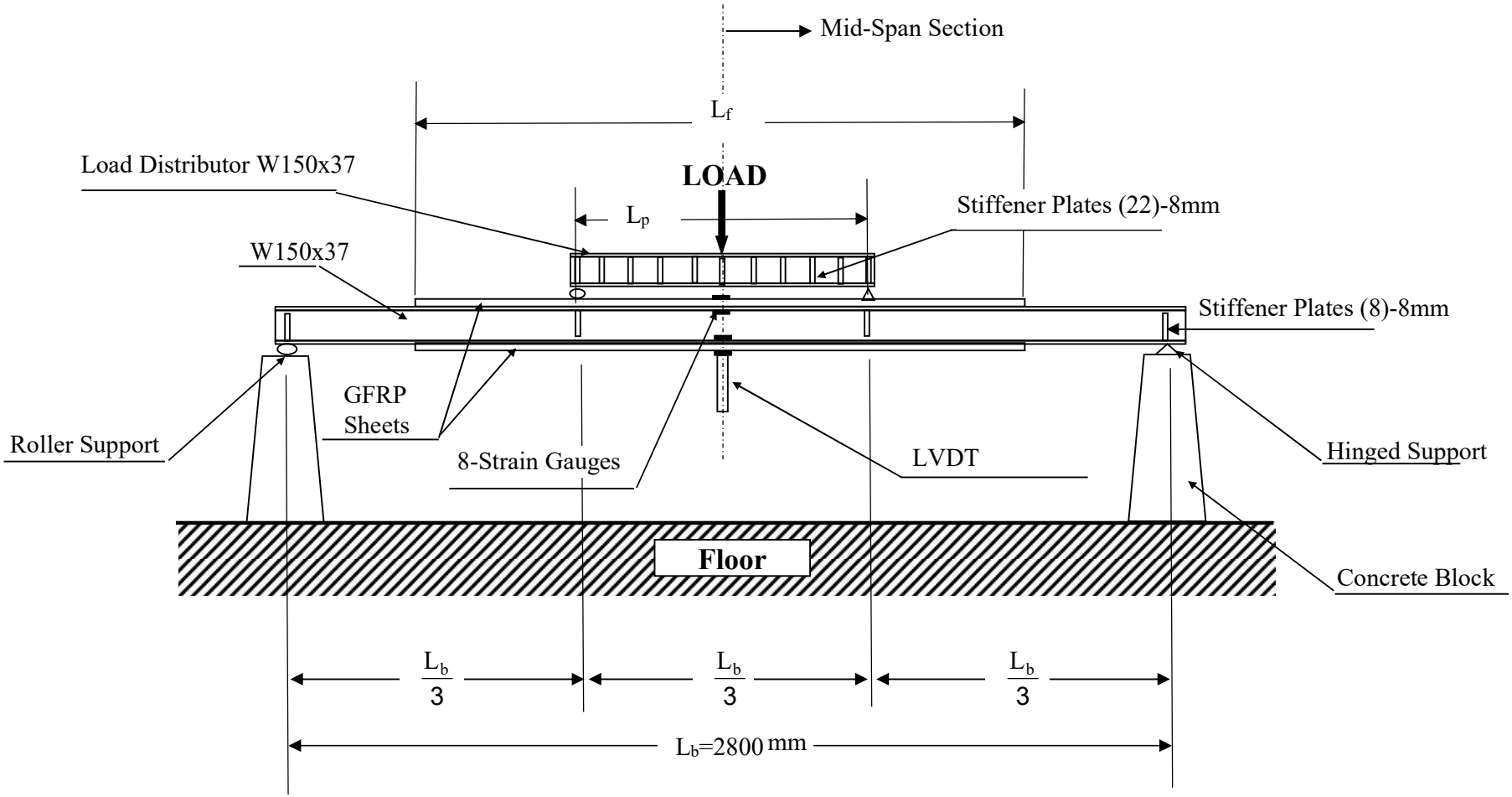

Figure 2a Schematic of Test Setup

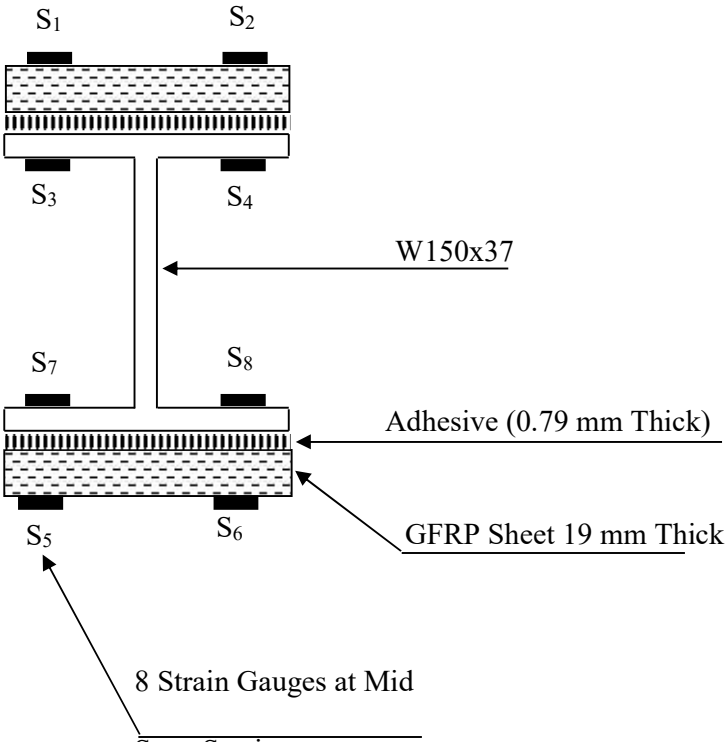

Figure 2b Cross Section of the Specimen

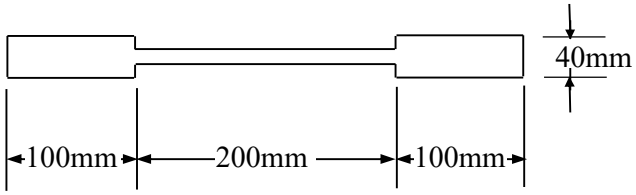

Figure 2c Steel Coupon Dimensions

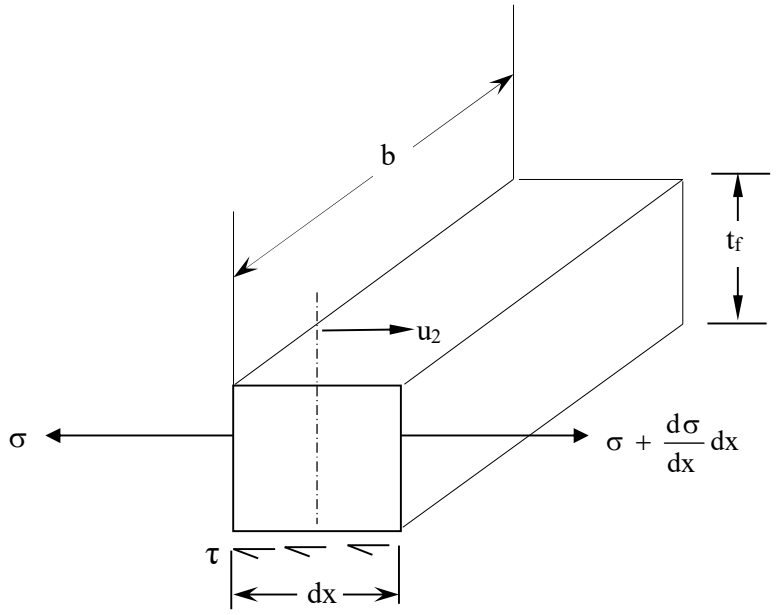

Figure 3a Stresses Acting on an Infinitesimal Element (dx) of the GFRP Plate

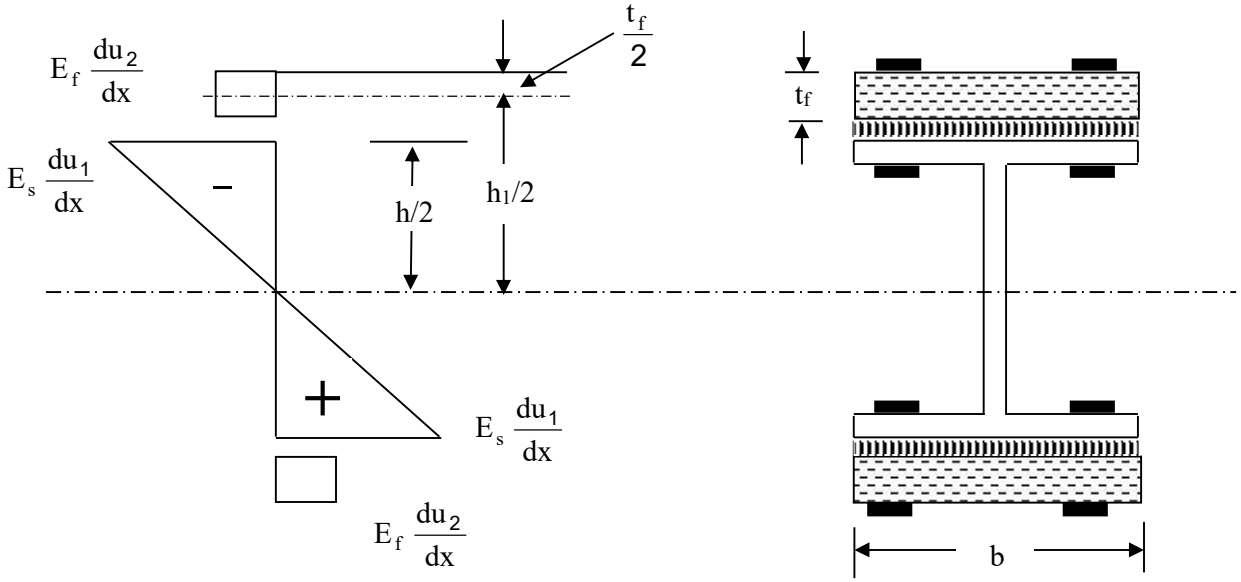

Figure 3b Typical Distribution of Axial Stress along the Depth of the Steel/ GFRP Section

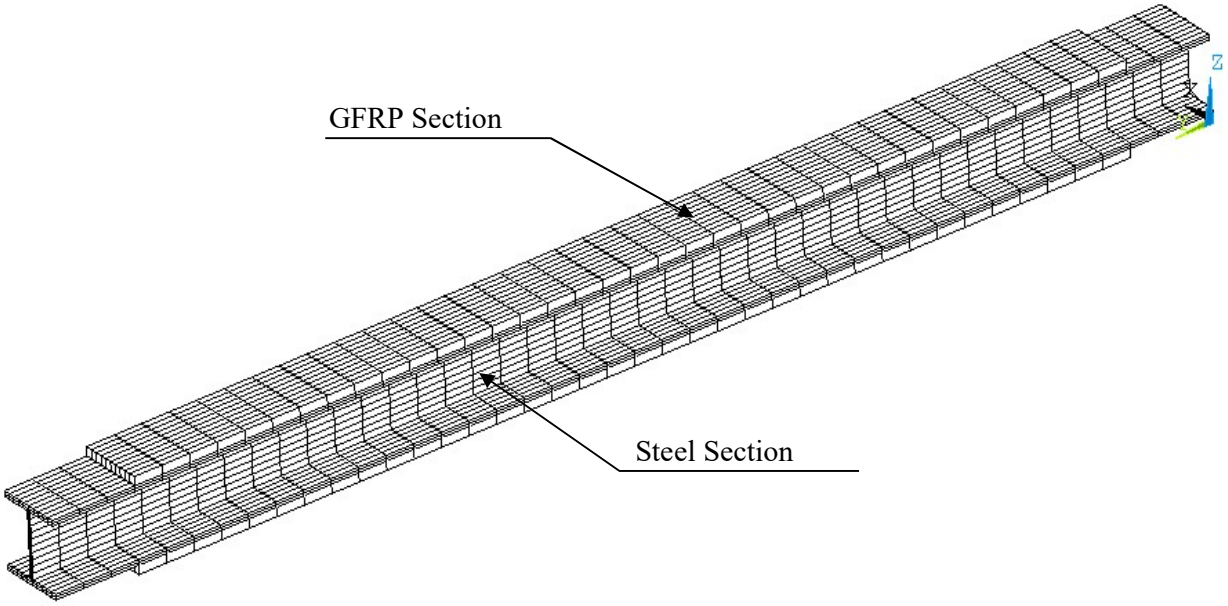

Figure 4 Typical Finite Element Mesh for the Rehabilitated Beam

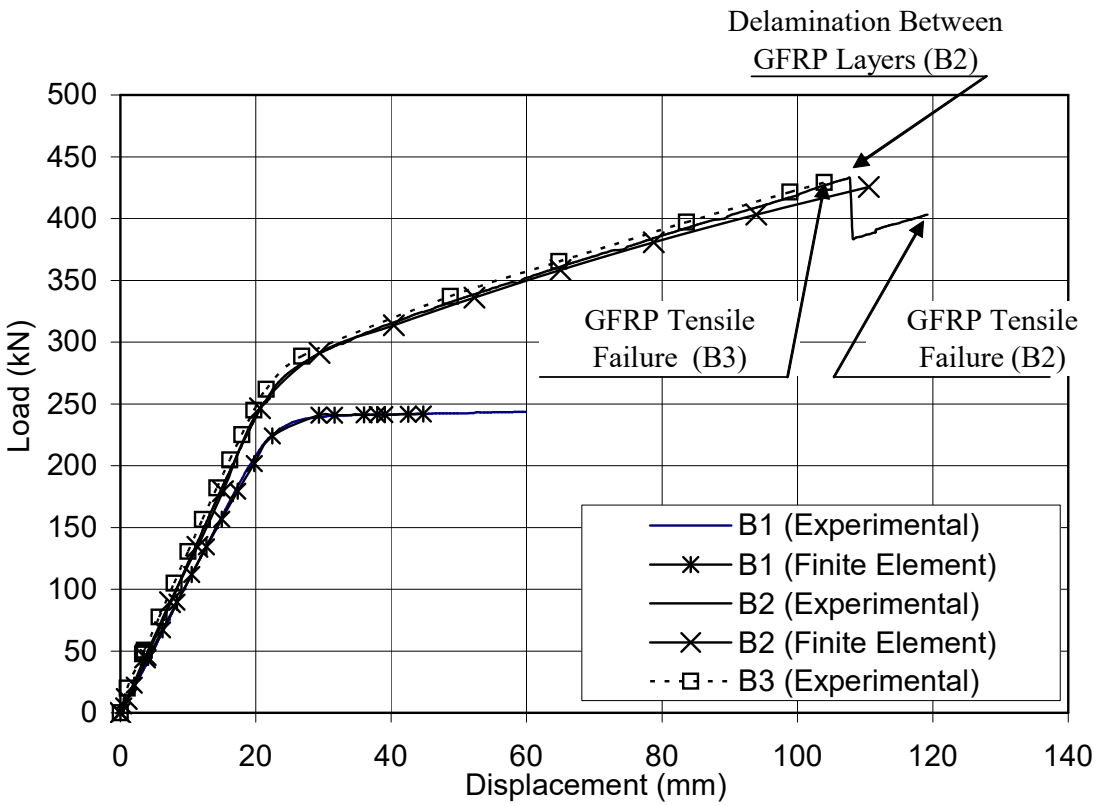

Figure 5 Load- Displacement Curve

Figure 6 Failure of Rehabilitated Steel Beam

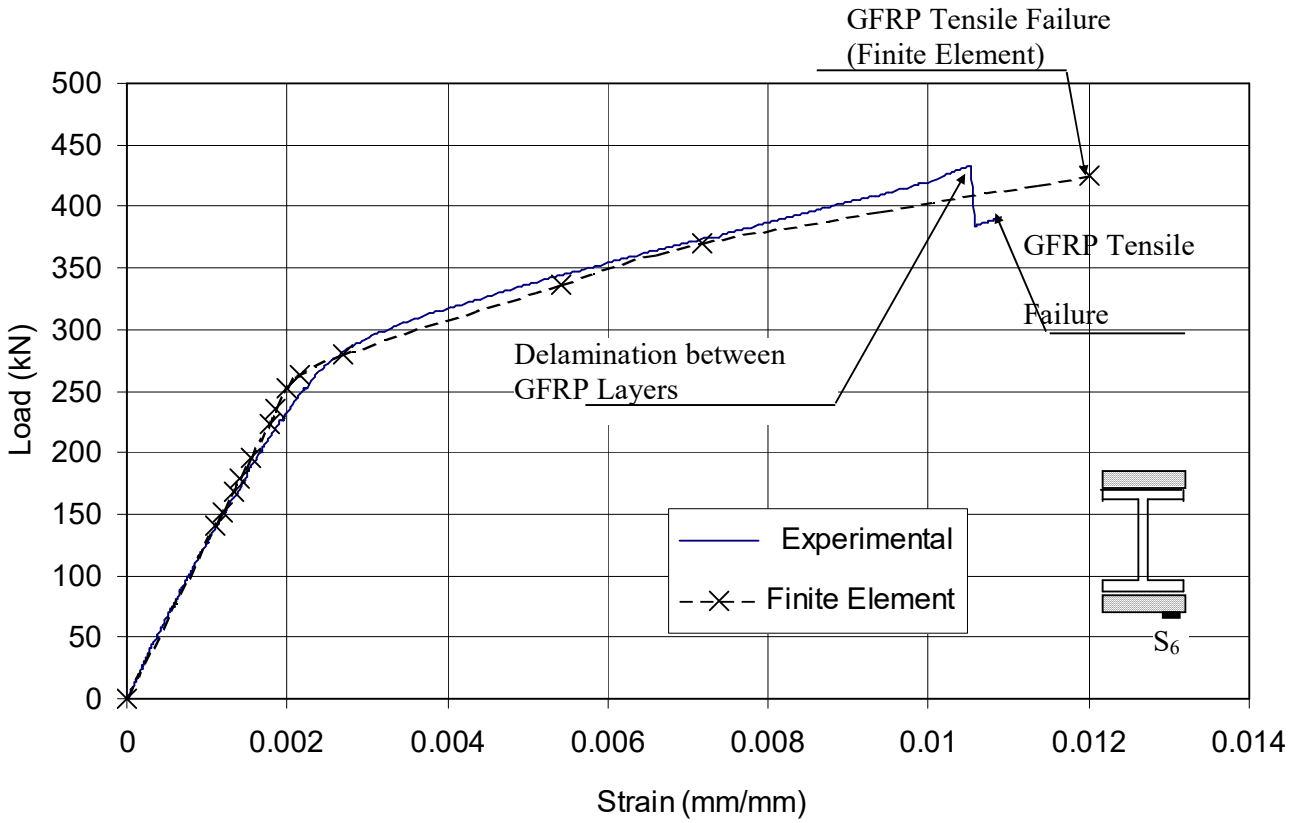

Figure 7a Rehabilitated Beam (B2): Load Strain Relationship Recorded by Strain Gauge S_6

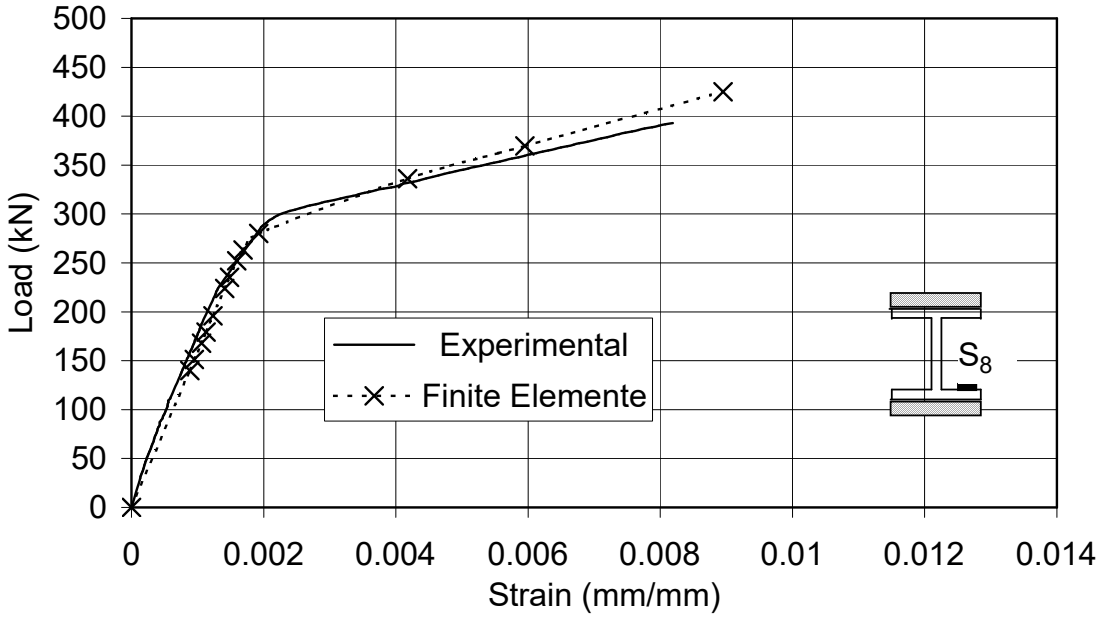

Figure 7b Rehabilitated Beam (B2): Load-Strain Relationship Recorded by Strain gauge S_8

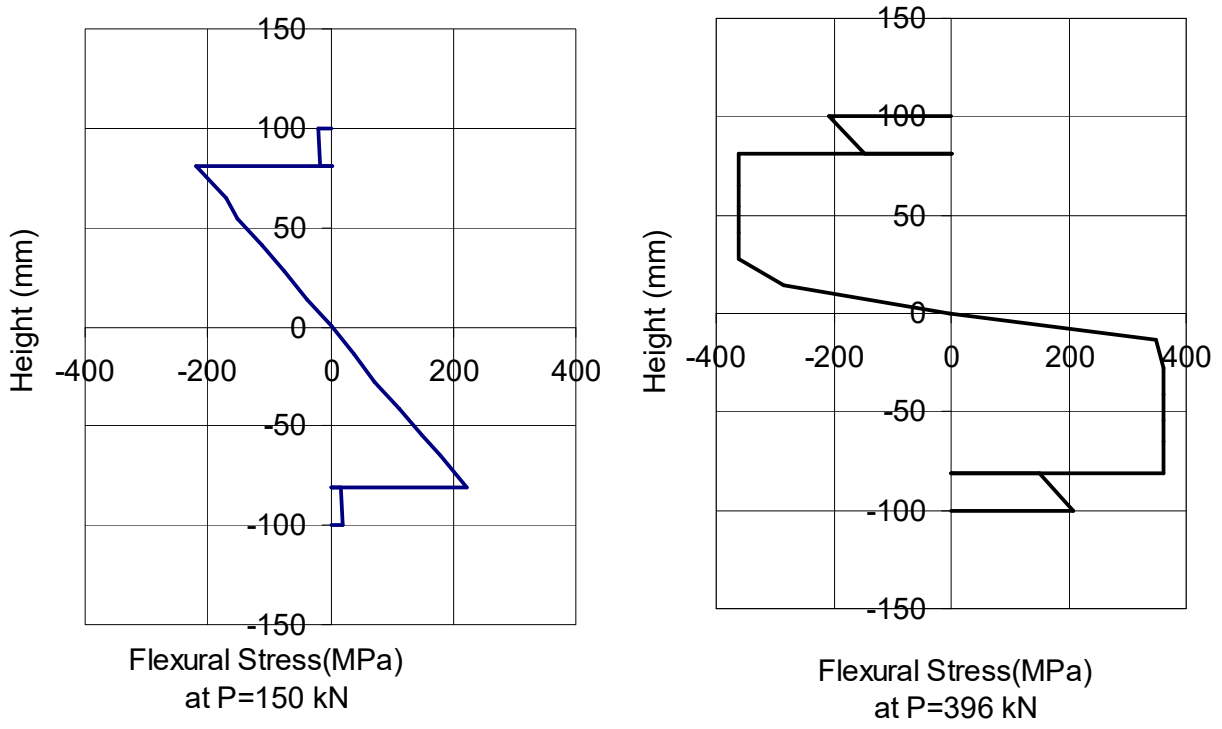

Figure 8 Flexural Stresses at Mid-Span Section of Rehabilitated Beam

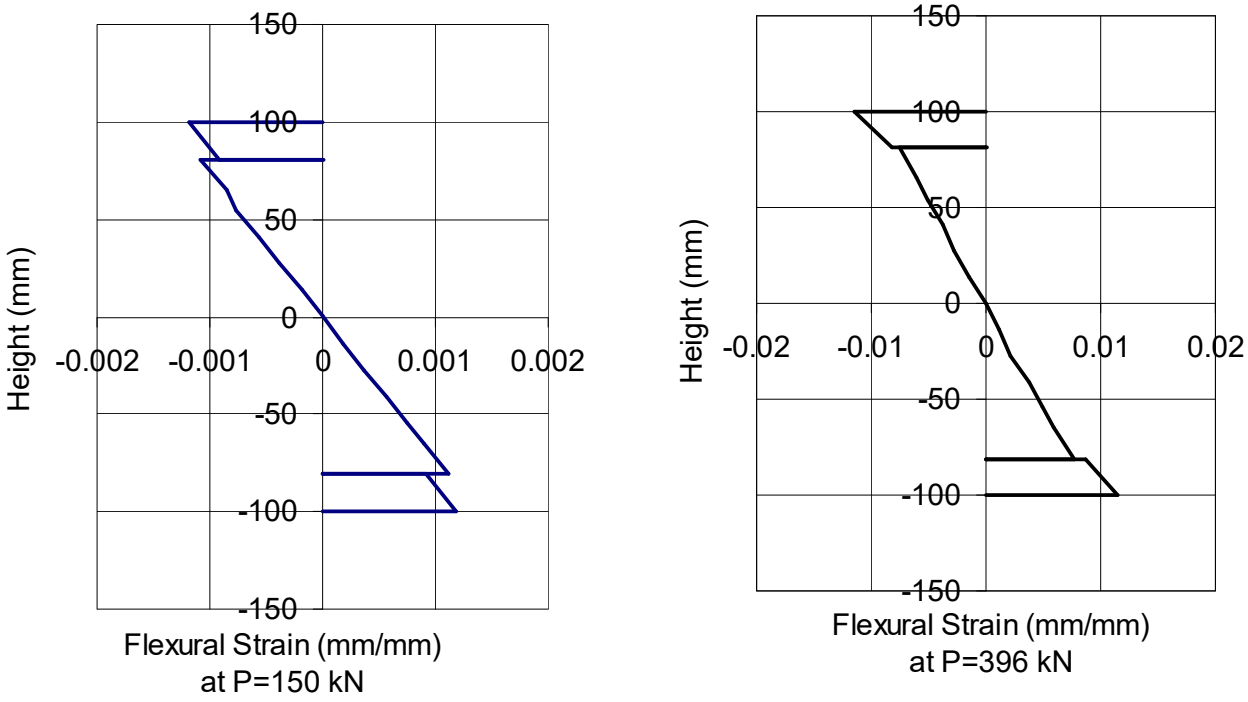

Figure 9 Flexural Stains at Mid-Span of Rehabilitated Beam

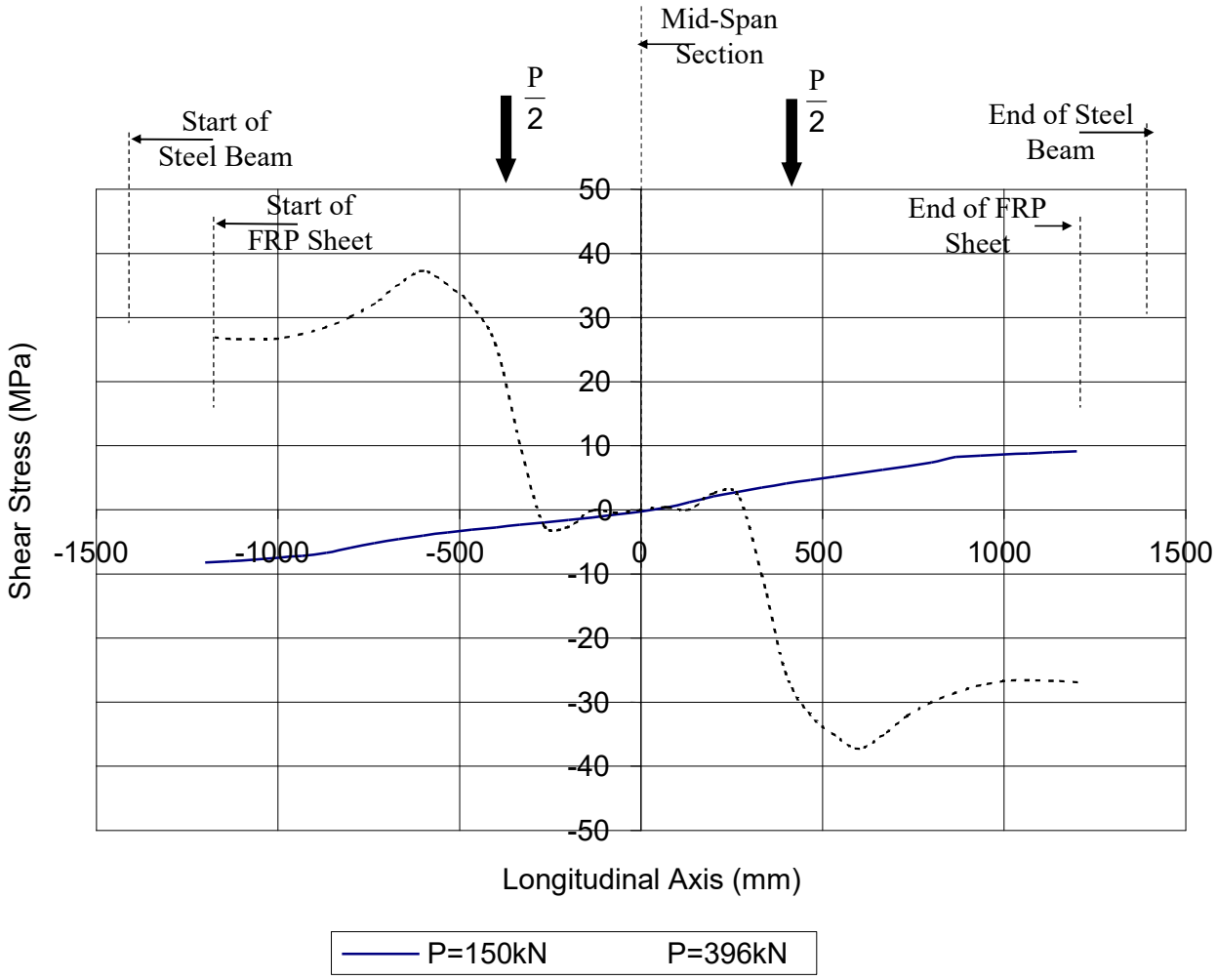

Figure 10 Longitudinal Shear-Stress Distribution for the Adhesive Connecting the Bottom Flange and the GFRP Sheet

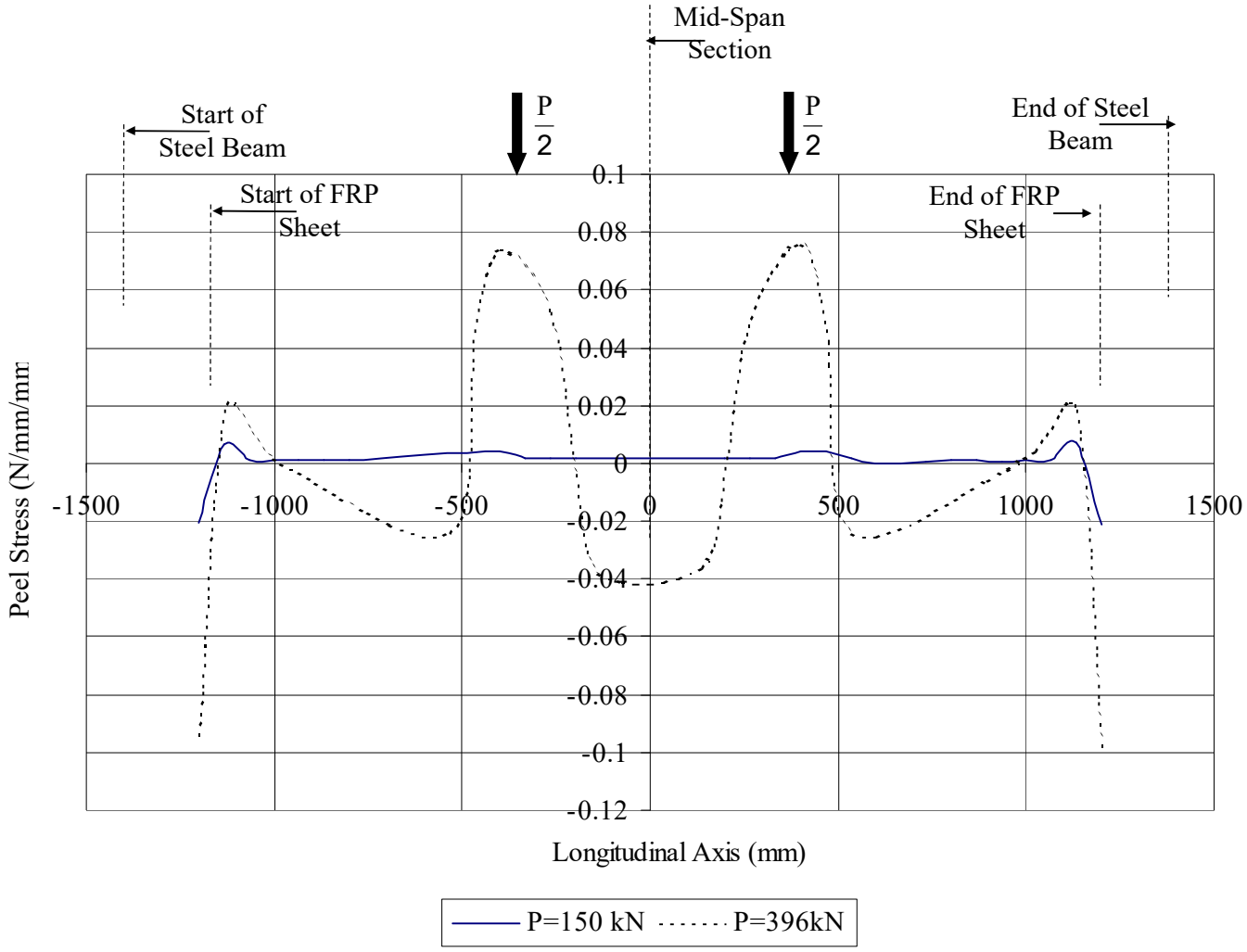

Figure 11 Longitudinal Peel-Stress Distribution for the Adhesive Connecting the Bottom Flange and the GFRP Sheet

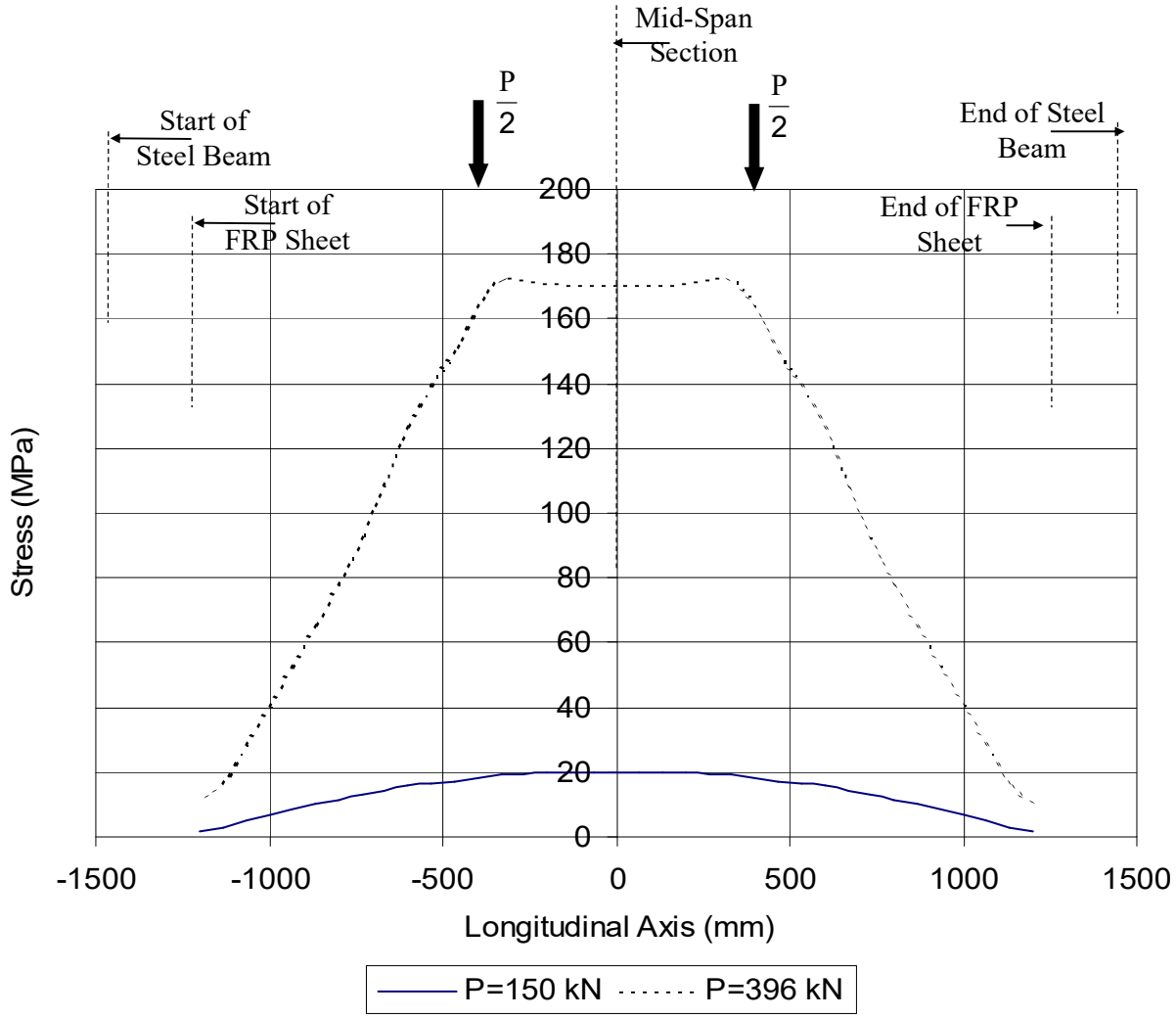

Figure 12 Bottom GFRP Sheet Longitudinal Axial Stress Distribution